Variable Ranking with PCA: Finding Multiparametric MR Imaging Markers for Prostate Cancer Diagnosis and Grading

Shoshana Ginsburg[1], Pallavi Tiwari[1], John Kurhanewicz[2], and Anant Madabhushi[1,⋆]

[1] Department of Biomedical Engineering, Rutgers University, USA
srosskam@eden.rutgers.edu, pallavit@eden.rutgers.edu, anantm@rci.rutgers.edu
[2] Department of Radiology, University of California, San Francisco, USA

Abstract. Although multiparametric (MP) MRI (MP–MRI) is a valuable tool for prostate cancer (CaP) diagnosis, considerable challenges remain in the ability to quantitatively combine different MRI parameters to train integrated, fused meta–classifiers for *in vivo* disease detection and characterization. To deal with the large number of MRI parameters, dimensionality reduction schemes such as principal component analysis (PCA) are needed to embed the data into a reduced subspace to facilitate classifier building. However, while features in the embedding space do not provide physical interpretability, direct feature selection in the high–dimensional space is encumbered by the curse of dimensionality. The goal of this work is to identify the most discriminating MP–MRI features for CaP diagnosis and grading based on their contributions in the reduced embedding obtained by performing PCA on the full MP–MRI feature space. In this work we demonstrate that a scheme called variable importance projection (VIP) can be employed in conjunction with PCA to identify the most discriminatory attributes. We apply our new PCA–VIP scheme to discover MP–MRI markers for discrimination between (a) CaP and benign tissue using 12 studies comprised of T2–w, DWI, and DCE MRI protocols and (b) high and low grade CaP using 36 MRS studies. The PCA–VIP score identified ADC values obtained from Diffusion and Gabor gradient texture features extracted from T2–w MRI as being most significant for CaP diagnosis. Our method also identified 3 metabolites that play a role in CaP detection—polyamine, citrate, and choline—and 4 metabolites that differentially express in low and high grade CaP: citrate, choline, polyamine, and creatine. The PCA–VIP scheme offers an alternative to traditional feature selection schemes that are encumbered by the curse of dimensionality.

⋆ Thanks to funding agencies: the Wallace H. Coulter Foundation, National Cancer Institute (R01CA136535-01, R01CA140772-01, R03CA143991-01), The Cancer Institute of New Jersey, The Society for Imaging Informatics in Medicine, the Department of Defense (W81XWH-09), and Rutgers University Presidential Fellowship.

A. Madabhushi et al. (Eds.): Prostate Cancer Imaging 2011, LNCS 6963, pp. 146–157, 2011.

1 Introduction

Prostate cancer (CaP), the second leading cause of cancer–related deaths among men [1], is typically diagnosed by a sextant trans–rectal ultrasound evaluation. Nevertheless, sensitivity of this diagnostic method is very poor due to the low resolution provided by ultrasound [2]. As a result, clinicians have explored employing T2–w MRI [3] and magnetic resonance spectroscopy (MRS) imaging [4] for CaP diagnosis and grading. While multiparametric (MP) MRI (MP–MRI) holds great promise for CaP diagnosis [4, 5, 6], there remains a need to identify the most discriminating imaging markers for identifying aggressive CaP *in vivo*, to assist clinicians in understanding the underlying disease processes and empower patients in deciding whether to pursue treatment or follow a watch–and–wait policy [7].

Furthermore, CaP diagnosis on MP–MRI is associated with high interobserver variability [8, 9]. For example, while metabolic concentrations of citrate, creatine, and choline present in MRS imaging have been shown to be linked to CaP presence and Gleason grade [4], the citrate and creatine peaks are often difficult to distinguish on MRS, resulting in inconsistent measurements by different observers [10]. In order to increase accuracy and reproducibility of CaP detection and grading on MP–MRI, researchers have turned to automated machine learning approaches to build integrated, fused classifiers that quantitatively combine multiple MRI parameters [11, 12, 13, 14, 15].

Nevertheless, building classifiers in high–dimensional spaces is encumbered by the curse of dimensionality [16]. Consequently, dimensionality reduction schemes such as principal component analysis (PCA) are needed to embed the data in a lower dimensional space where classification can be performed. While PCA–based classifiers provide substantial benefit for combining multiple MRI parameters to build integrated meta–classifiers [17], PCA does not allow for easy identification of the features in the original, high–dimensional space that are most relevant for classification [18]. At the same time, feature selection schemes that identify important features in the original space are often limited by dependencies and interactive effects among features [19]. Hence, there remains a need for methods to identify features that contribute most to PCA embeddings.

In this work we present an innovative scheme for computing a measure of variable importance in projections (VIP) that considers both the structure of the reduced dimensional PCA embedding and the class labels. Thus, the VIP method scores features based on the significance of their contributions in the PCA embedding where classifiers can be built. Whereas the concept of VIP exists for partial least squares [20], in this work we demonstrate that VIP can be extended in the context of PCA as well. Unlike other feature selection schemes, PCA–VIP is not encumbered by the curse of dimensionality because the most contributory features are identified in the reduced embedding space.

In this work we apply PCA–VIP to identify MP–MRI markers to distinguish between (a) benign tissue and CaP on 12 T2–w, DWI, and DCE MRI studies and (b) low and high grade CaP on 22 MRS studies. The former dataset has ground truth annotation of spatial extent of CaP *in vivo*, and the latter has

ground truth annotation of both diagnosis and spatial extent of CaP *in vivo*. Our methodology comprises the following main steps. First PCA is applied to the MP–MRI features, which include spectral peaks on MRS and texture features on MRI, at the voxel level. PCA–VIP scores are assigned to the high–dimensional features, and the high–dimensional features with the highest PCA–VIP scores are identified. The PCA–VIP scheme is then evaluated via a classifier trained using the features with high PCA–VIP scores. The performance of this classifier is then compared against one that operates in the full high–dimensional space, the hypothesis being that the lack of statistically significant differences between the two classifiers will reflect that only the most class discriminatory attributes are being identified via PCA–VIP.

The remainder of this paper is organized as follows. In Section 2 we discuss PCA and how variable importance is determined by PCA–VIP. We apply our PCA–VIP methodology in Section 3 to identify MP–MR imaging markers for discrimination of (a) benign tissue and CaP and (b) high and low grade CaP on MP–MRI, and in Section 4 we provide some concluding remarks.

2 Variable Importance in Projection for PCA

2.1 Principal Component Analysis

PCA [21] attempts to find a linear transformation to maximize the variance in the data and applies this transformation to obtain the most uncorrelated features. The orthogonal eigenvectors of the data matrix $\mathbf{X}$ express the variance in the data, and the h eigenvectors that comprise most of the variance in the data are the principal components. Thus, PCA forms the following model:

$$\mathbf{X} = \mathbf{T}\mathbf{P}^{\mathsf{T}}, \tag{1}$$

where $\mathbf{T}$ is made up of the h principal component vectors $\mathbf{t}_i$, $i \in \{1, ..., h\}$, as columns and $\mathbf{P}^{\mathsf{T}}$ is comprised of the h loading vectors $\mathbf{p}_i$ as rows.

2.2 Variable Importance in PCA Projections

The features that contribute most to the i^{th} dimension of the PCA transformation can be identified as those with the largest weights in the i^{th} loading vector; the fraction $\left(\frac{p_{ji}}{||\mathbf{p}_i||}\right)^2$ reveals how much the j^{th} feature contributes to the i^{th} principal component in the low–dimensional embedding. The overall importance of the jth feature to classification can be calculated by summing its contribution to each dimension of the PCA embedding and weighting these values by (a) the regression coefficients b_i, which relate the data back to the class labels, and (b) the transformed data $\mathbf{t}_i$. Thus, although PCA is itself an unsupervised method, the exploitation of class labels in computing the PCA–VIP leads to the identification of features that provide good class discrimination. The variable importance in projections (VIP) for PCA (PCA–VIP) is computed for each feature as follows:

$$\pi_j = \sqrt{m \frac{\sum_{i=1}^{h} b_i^2 \mathbf{t}_i^\mathsf{T} \mathbf{t}_i \left(\frac{p_{ji}}{||\mathbf{p}_i||}\right)^2}{\sum_{i=1}^{h} b_i^2 \mathbf{t}_i^\mathsf{T} \mathbf{t}_i}}, \tag{2}$$

where m is the number of features in the original, high–dimensional feature space, and the b_i are the coefficients that solve the regression equation

$$\mathbf{y} = \mathbf{T}\mathbf{b}^\mathsf{T}, \tag{3}$$

which correlates the principal components with the outcome vector $\mathbf{y}$. The degree to which a feature contributes to classification in the PCA transformed space is directly proportional to its associated PCA–VIP scores. Thus, features with PCA–VIP scores near 0 have little predictive power, and the features with the highest PCA–VIP scores contribute the most to class discrimination on the PCA embedding.

3 Experimental Results and Discussion

3.1 Identification of Imaging Markers for CaP Diagnosis

Data. A total of 12 pre–operative, endorectal *in vivo* 3 Tesla MR imaging studies including T2–w, DWI, and DCE MRI in men with organ confined prostate cancer were obtained prior to radical prostatectomy. Surgical specimens were then sectioned and examined by a trained pathologist to accurately delineate CaP presence and extent. Registration of multimodal imagery with histology was performed using Multiple–Attribute Combined Mutual Information (MACMI) [22], a non–rigid registration scheme that performs non–linear image warping at multiple image scales via a hierarchical B–spline mesh grid optimization scheme. 39 corresponding histological sections were brought into spatial alignment with corresponding T2–w, DWI, and DCE MRI slices to determine ground truth spatial extent of CaP on MRI.

Feature Extraction. A series of 18 voxel–wise image features, including six features from each of the T2–w, DWI, and DCE MRI protocols, were extracted from each of the 39 MP–MRI slices for discrimination between benign tissue and CaP. For each voxel on the T2–w and DCE MRI slices three co–occurrence features (contrast inverse moment, contrast average, and correlation), the magnitude gradient, and a Gabor feature combining all orientations of the Gabor filter via the l_∞ norm were extracted [14]. Additionally, the T2–w and ADC intensity values were taken as the sixth feature for each protocol. The six features extracted from DCE MRI were the post–contrast intensity values at each time point.

Table 1. Description of MP–MRI datasets used for CaP diagnosis and grading. Contributory features, as well as their associated PCA–VIP scores, are listed for each MRI protocol: T2–w, DWI, DCE, and MRS. Standard deviation of performance measures obtained by boot–strapping are shown in parentheses, and the feature from each MRI protocol with the highest PCA–VIP score is shown in bold.

MRI Protocol	Classes	Contributory Features	PCA–VIP
T2–w MRI	benign/CaP (12 studies)	**Gabor gradient**	1.63(0.002)
		Intensity value	.962(0.029)
DCE MRI	benign/CaP (12 studies)	**Time point 2**	1.56(0.002)
		Time point 6	.987(0.001)
ADC MRI	benign/CaP (12 studies)	**Intensity value**	2.27(0.002)
		Gabor gradient	1.82(0.019)
MRS	benign/CaP (22 studies)	**Polyamine**	2.92(0.137)
		Citrate	2.27(0.116)
		Choline	1.88(0.364)
		Creatine	1.04(0.216)
MRS	low/high grade (9 studies)	**Citrate**	2.18(0.107)
		Choline	2.14(0.113)
		Polyamine	2.13(0.130)
		Creatine	2.09(0.106)

MP–MR Imaging Marker Identification. CaP detection on MP–MRI was performed by representing each voxel within the prostate by the 18 extracted features and transforming this voxel–wise data using PCA. PCA–VIP scores were then calculated by boot–strapping for each of the 18 features. Randomized boot–strapping was performed by randomly selecting 8 of the 12 patient studies to obtain a PCA embedding and compute the PCA–VIP scores therewith. This randomized boot–strapping process was repeated 50 times, and the average values and standard deviatons of PCA–VIP scores were obtained from boot–strapping. Features associated with high PCA–VIP scores were identified as imaging markers for CaP diagnosis.

Evaluation. The probabilistic boosting tree (PBT) [25], which iteratively generates a decision tree structure of a predefined size and whose nodes combine classifier predictions from several weak classifiers, was employed to construct C^{all}, a classifier using all 18 features, and C^{VIP}, a classifier using the four features associated with the highest PCA–VIP scores. Since PBTs necessitate the use of atleast two features, this classifier could not be used to evaluate individual feature performance. Consequently, the naive Bayes classifier [26] was employed to construct classifiers $C^1, ..., C^4$ using each of the four features used in C^{VIP}.

Performance of each of C^1, C^2, C^3, C^4, C^{all}, and C^{VIP} was evaluated by accuracy and AUC estimates obtained via cross–validation, which was done by performing classification of each prostate voxel in the 12 studies. For each of the 12 studies, six classifiers—C^{all}, C^{VIP}, and C^k, $k \in \{1, ..., 4\}$—were trained on a

random selection of 9 other studies, and each voxel in the prosate was classified as benign or CaP by each classifier. This process was repeated 50 times, and the average values and standard deviations of the performance measures over the 50 iterations were obtained for each of the six classifiers.

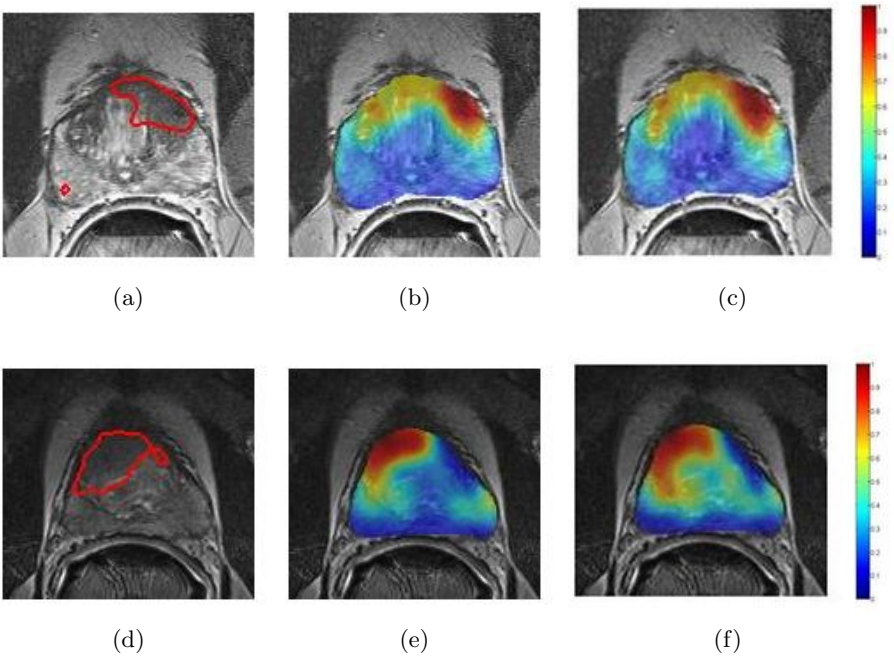

Fig. 1. Sample prostate T2–w MRI slices in (a) and (d) have CaP ground truth shown in red. Heat map representations of the probabilities that voxels within the prostate contain CaP are shown in (b) and (e) when C^{all} is used for classification and in (c) and (f) when C^{VIP} is used for classification. Red voxels denote high probability of CaP, while cool colors denote high probability that a voxel corresponds to benign tissue. The probability maps in (b) and (e) are similar to (c) and (f), respectively, demonstrating that eliminating features with low PCA–VIP scores does not significantly impact overall classifier performance.

Results and Discussion. PCA–VIP scores obtained for each of the 18 image features are shown in Table 1. The Gabor gradient features [23] extracted from both the T2–w MRI and ADC maps emerge as contributory to the PCA embedding for discriminating benign and CaP regions. The importance of Gabor wavelet features lies in their ability to quantify the visual appearance of CaP, typically documented by radiologists as a region of low signal intensity with incomplete stromal septations within its focus (on T2–w MRI). The Gabor operator attempts to match such localized frequency characteristics across

multiple scales and orientations, allowing quantification of features that are used in visual processing [24]. Additional features whose importance is revealed by the PCA–VIP score are the ADC and the DCE intensity value at the second time point, which corresponds to peak enhancement (see Table 1). In fact, it is visually apparent on MRI that CaP voxels tend to have significantly lower ADC values and quicker contrast enhancement on DCE compared to benign voxels.

Table 2. Classification performance for C^{all}, C^{VIP}, C^1, C^2, C^3, and C^4 for CaP diagnosis on T2–w/DWI/DCE MRI. Standard deviation of performance measures from the 50 iterations are shown in parentheses.

	C^{all}	C^{VIP}	C^1	C^2	C^3	C^4
Accuracy	0.78(0.007)	0.78(0.006)	0.57(0.010)	0.47(0.007)	0.65(0.007)	0.49(0.013)
AUC	0.64(0.011)	0.64(0.011)	0.63(0.007)	0.53(0.009)	0.59(0.006)	0.55(0.014)

Qualitative results, displayed in Figure 1, illustrate that classification does not change significantly when features with low PCA–VIP scores are eliminated from the classification model. Quantitative results (see Table 2) confirm that classification accuracy and AUC are similar for C^{all} and C^{VIP}. The fact that classifier performance is not weakened significantly when C^{VIP} is used instead of C^{all} suggests that most of the relevant information captured by the 18 extracted features is contained within these four features. The results shown in Table 2 also indicate that combining the four features with high PCA–VIP scores provides for greater classification accuracy than using any of the features individually for classification.

3.2 Identifying Imaging Markers for CaP Grading

Data. A total of 22 pre–operative, endorectal *in vivo* 3 Tesla T2–w MRI, MRS studies were obtained. Upon radical prostatectomy, "ground truth" CaP extent and grade were manually delineated by an expert by visually registering corresponding histological and radiological sections. Class labels for the individual spectral voxels, assigned via a combination of manual registration of histology and MRI and subsequent expert inspection, were used as the surrogate ground truth for CaP detection and grading. The 22 studies comprised a total of 794 CaP and 1056 benign voxels, and 9 of these studies were found to contain 179 low grade CaP voxels and 231 high grade CaP voxels. Each voxel is associated with a 171–dimensional spectral vector, which encodes the metabolic concentrations of choline, polyamine, creatine, and citrate.

Feature Extraction. Three–dimensional MRS imaging data were processed and aligned with the corresponding T2–w imaging data. The raw spectral data was filtered with a 3 Hz Gaussian filter, Fourier transformed, baseline corrected, and phase and frequency aligned based upon the water peak using the methods in [27, 28]. Post baseline and frequency correction, choline, polyamine, creatine, and citrate peak areas were estimated using the composite trapezoidal rule [29].

MP–MR Imaging Marker Identification. Metabolic imaging markers that contribute to accurate diagnosis and Gleason grading of CaP spectra on MRS were identified by representing each voxel within the prostate by the 171 spectral features and transforming this voxel–wise data using PCA. PCA–VIP scores were then calculated by boot–strapping for each of the 171 spectral features. Randomized boot–strapping was performed by randomly selecting 16 of the 22 patient studies (or 6 of the 9 patient studies with Gleason grade information) to obtain a PCA embedding. This randomized boot–strapping process was repeated 50 times, and the average values and standard deviatons of PCA–VIP scores were obtained from boot–strapping. Dominant metabolites were found by aligning PCA–VIP score curves (see Figure 2(a)) with the spectral vectors and identifying spectral peaks with the highest PCA–VIP scores.

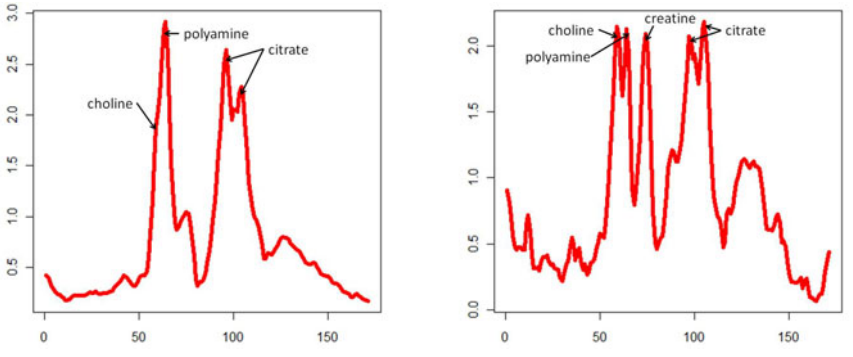

Fig. 2. PCA–VIP score curves for MRS spectra for discriminating between (a) benign tissue and CaP and (b) low and high grade CaP. Choline, polyamine, and citrate peaks emerge as contributory in classifying benign tissue and CaP, and choline, polyamine, creatine, and citrate differentially express in low and high grade CaP.

Evaluation. PBTs were employed to construct C^{all}, a classifier using all 171 spectral features, and C^{VIP}, a classifier using the peaks associated with the highest PCA–VIP scores. The naive Bayes classifier was employed to construct classifiers $C^1, ..., C^4$ using each of the peaks used in C^{VIP}. Classification performance was evaluated by accuracy and AUC estimates obtained via cross–validation. The average values and standard deviations of the performance measures over the 50 iterations are reported for C^{all}, C^{VIP}, C^1, C^2, C^3, and C^4.

Results and Discussion. PCA–VIP scores, shown in Figure 2, suggest that choline, polyamine, and citrate play a significant role in discrimination between CaP and benign tissue and that these three metabolities, as well as creatine, aid in differentiation of low and high grade CaP. Our results confirm the roles

Table 3. Classification performance for C^{all}, C^{VIP}, C^1, C^2, C^3, and C^4 for CaP diagnosis on MRS. Standard deviation of performance measures from the 50 iterations are shown in parentheses.

	$C^{\mathbf{all}}$	$C^{\mathbf{VIP}}$	C^1	C^2	C^3
Accuracy	0.78(0.001)	0.78(0.002)	0.69(0.002)	0.70(0.001)	0.70(0.002)
AUC	0.86(0.008)	0.74(0.008)	0.49(0.014)	0.56(0.014)	0.54(0.019)

of choline and citrate for CaP detection and grading of prostate, previously suggested in [4]. We find that although creatine is not a significant contributor to CaP detection, creatine appears to play an important role in differentiating between high and low grade CaP.

Table 4. Classification performance for C^{all}, C^{VIP}, C^1, C^2, C^3, and C^4 for CaP grading on MRS. Standard deviation of performance measures from the 50 iterations are shown in parentheses.

	$C^{\mathbf{all}}$	$C^{\mathbf{VIP}}$	C^1	C^2	C^3	C^4
Accuracy	0.72(0.043)	0.71(0.034)	0.58(0.062)	0.61(0.045)	0.56(0.069)	0.60(0.050)
AUC	0.76(0.061)	0.74(0.070)	0.54(0.107)	0.65(0.053)	0.60(0.090)	0.64(0.051)

Furthermore, PCA–VIP also reveals the importance of polyamine concentrations in distinguishing both CaP and benign tissue and low and high grade CaP. Low polyamine concentration was previously linked to CaP presence [4], and Swanson et. al. [30] suggested that cancer aggressiveness was associated with further reduction of polyamines. However, the number of cancerous samples in the Swanson study was small, so the findings could not be verified as being statistically significant. The results of this study strongly suggest that polyamine concentrations are differentially expressed in low and high grade CaP.

To quantitatively evaluate the discriminability of the metabolite features identified as important via PCA–VIP, PBT classifiers using only these metabolic concentrations were constructed to classify the individual spectra. Qualitative results, displayed in Figure 3 for discrimination between high and low grade spectra, illustrate higher sensitivity for C^{VIP} compared to C^{all}. Quantitative results (see Tables 3 and 4) confirm that both accuracy and AUC are similar for C^{VIP} and C^{all} for the CaP grading problem. For CaP diagnosis, C^{VIP} had a slightly lower AUC than C^{all}, suggesting that perhaps other, yet to be identified metabolites contribute to CaP–benign class separability. The results shown in Tables 3 and 4 also indicate that combining the peaks associated with high PCA–VIP scores provides for greater classification accuracy than using any of the metabolic peaks individually.

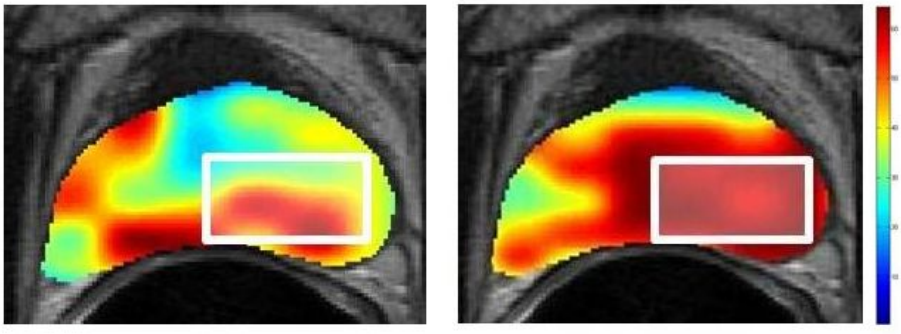

(a) (b)

Fig. 3. Heat map representations of the probabilities that voxels within the prostate correspond to high grade CaP when (a) C^{all} and (b) C^{VIP} were used for classification. Ground truth presence of high grade CaP is shown within the white rectangles.

4 Concluding Remarks

We presented the PCA–VIP scheme, which facilitates interpretation of PCA models by quantifying the contributions of individual features on PCA embeddings. We demonstrated how PCA–VIP enables identification of imaging markers for CaP detection and grading on MP–MRI. The ability of PCA–VIP to correctly identify features that contribute to class discrimination was corroborated by the fact that classifier performance was largely unaffected by the elimination of features with low PCA–VIP scores. The work presented here could potentially be used for modulating the time and complexity of the prostate imaging exam by limiting the imaging acquisition to only those parameters found to be relevant.

Whereas traditional feature selection algorithms operate in the high dimensional feature space and are therefore encumbered by the curse of dimensionality, the PCA–VIP provides a means for feature selection, ranking, and weighting in the PCA embedding space. In future work we intend to explore the application of this scheme to other problem domains.

References

[1] Jemal, A., et al.: Cancer Statistics. CA Cancer Journal for Clinicians 60(5), 277–300 (2010)

[2] Borboroglu, P.G., et al.: Extensive repeat transrectal ultrasound guided prostate biopsy in patients with previous benign sextant biopsies. The Journal of Urology 163(1), 158–162 (2000)

[3] Schiebler, M.L., et al.: Current role of MR imaging in the staging of adenocarcinoma of the prostate. Radiology 189(2), 339–352 (1993)

[4] Kurhanewicz, J., et al.: Combined magnetic resonance imaging and spectroscopic imaging appraoch to molecular imaging of prostate cancer. Journal of Magnetic Resonance Imaging 16, 451–463 (2002)

[5] Shukla–Dave, A., et al.: The utility of magnetic resonance imaging and spectroscopy for predicting insignificant prostate cancer: An initial analysis. BJU International 99, 786–793 (2007)
[6] Langer, D.L., et al.: Prostate tissue composition and MR measurements: Investigating the relationsips between ADC, T2, Ktrans, ve, and corresponding histological features. Radiology 255, 485–494 (2010)
[7] Klotz, L.: Active surveillance for prostate cancer: For whom? Journal of Clinical Oncology 23(32), 8165–8169 (2005)
[8] May, F., et al.: Limited value of endorectal magnetic resonance imaging and transrectal ultrasonography in the staging of clinically localized prostate cancer. BJU International 87(1), 66–69 (2001)
[9] Bonilla, J., et al.: Intra– and interobserver variability of MRI prostate volume measurements. Prostate 31(2), 98–102 (1997)
[10] Wetter, A., et al.: Combined MRI and MR spectroscopy of the prostate before radical prostatectomy. American Journal of Roentgenology 187, 724–730 (2006)
[11] Liu, X., et al.: Prostate cancer segmentation with simultaneous estimation of Markov random field parameters and class. IEEE Transactions on Medical Imaging 28(6), 906–915 (2009)
[12] Tiwari, P., et al.: A hierarchical spectral clustering and nonlinear dimensionality reduction scheme for detection of prostate cancer from magnetic resonance spectroscopy (MRS). Medical Physics 36(9), 3927–3939 (2009)
[13] Vos, P.C., et al.: Computer–assisted analysis of peripheral zone prostate lesions using T2–weighted and dynamic contrast enhanced T1–weighted MRI. Physics in Medicine and Biology 55(6), 1719 (2010)
[14] Viswanath, S., et al.: Enhanced multi–protocol analysis via intelligent supervised embedding (EMPrAvISE): Detecting prostate cancer on multi–parametric MRI. In: SPIE Medical Imaging, vol. 7963, pp.79630U
[15] Tiwari, P., et al.: Multimodal wavelet embedding representation for data combination (MaWERiC): Integrating magnetic resonance imaging and spectroscopy for prostate cancer detection. Accepted to: NMR in Medicine
[16] Duda, R., et al.: Pattern Classification, 2nd edn. Wiley-Interscience, Chichester (2000)
[17] Kelm, B.M., et al.: Automated estimation of tumor probability in prostate magnetic resonance spectroscopic imaging: Pattern recognition vs quantification. Magnetic Resonance in Medicine 57, 150–159 (2007)
[18] Craig, A., et al.: Scaling and normalization effects in NMR spectroscopic metabonomic data sets. Analytical Chemistry 78, 2262–2267 (2006)
[19] Yan, H., et al.: Correntropy based feature selection using binary projection. Pattern Recognition 44(12), 2834–2843 (2011)
[20] Chong, I.G., Jun, C.H.: Performance of some variable selection methods when multicollinearity is present. Chemometrics and Intelligent Laboratory Systems 78, 103–112 (2005)
[21] Esbensen, K.: Multivariate data analysis—in practice: An introduction to multivariate data analysis and experimental design. CAMO, Norway (2004)
[22] Chappelow, J., et al.: Elastic registration of multimodal prostate MRI and histology via multiattribute combined mutual information. Medical Physics 38, 2005–2018 (2011)
[23] Madabhushi, A., et al.: Automated detection of prostatic adenocarcinoma from high resolution ex vivo MRI. IEEE Transactions on Medical Imaging 24(12), 1611–1625 (2005)

[24] Bovik, A.C., et al.: Multichannel texture analysis using localized spatial filters. IEEE Transactions on Pattern Analysis and Machine Intelligence 12(1), 55–73 (1990)
[25] Quinlan, J.R.: C4.5: Programs for Machine Learning. Morgan Kaufmann, San Francisco (1993)
[26] Witten, I.H., Frank, E.: Data Mining: Practical Machine Learning Tools and Techniques. Elsevier, Amsterdam (2005)
[27] Nelson, S.J., Brown, T.: A new method for automatic quantification of 1–D spectra with low signal to noise ratio. Journal of Magnetic Resonance Imaging 84, 95–109 (1987)
[28] Nelson, S.J.: Analysis of volume MRI and MR spectroscopic imaging data for the evaluation of patients with brain tumors. Magnetic Resonance in Medicine 46, 228–239 (2001)
[29] Devos, A., et al.: Classification of brain tumours using short echo time 1H MR spectra. Journal of Magnetic Resonance 170(1), 164–175 (2004)
[30] Swanson, M.G., et al.: 1H HR–MAS investigation of four potential markers for prostate cancer. Proc. Intl. Soc. Mag. Reson. Med. 9 (2001)